Supplementary: "Absorption enhancement of BC particles in a Mediterranean city and countryside"

Jesús Yus-Díez[1,2], Marta Via[1,2], Andrés Alastuey[1], Angeliki Karanasiou[1], María Cruz Minguillón[1], Noemí Perez[1], Xavier Querol[1], Cristina Reche[1], Matic Ivančič[3], Martin Rigler[3], and Marco Pandolfi[1]

[1]Institute of Environmental Assessment and Water Research (IDAEA-CSIC), Barcelona, 08034, Spain
[2]Grup de Meteorologia, Departament de Física Aplicada, Universitat de Barcelona, C/Martí i Franquès, 1, 08028, Barcelona, Spain
[3]Aerosol d.o.o., Ljubljana, Slovenia

Correspondence: Jesús Yus-Díez (jesus.yus@idaea.csic.es) & Marco Pandolfi (marco.pandolfi@idaea.csic.es)

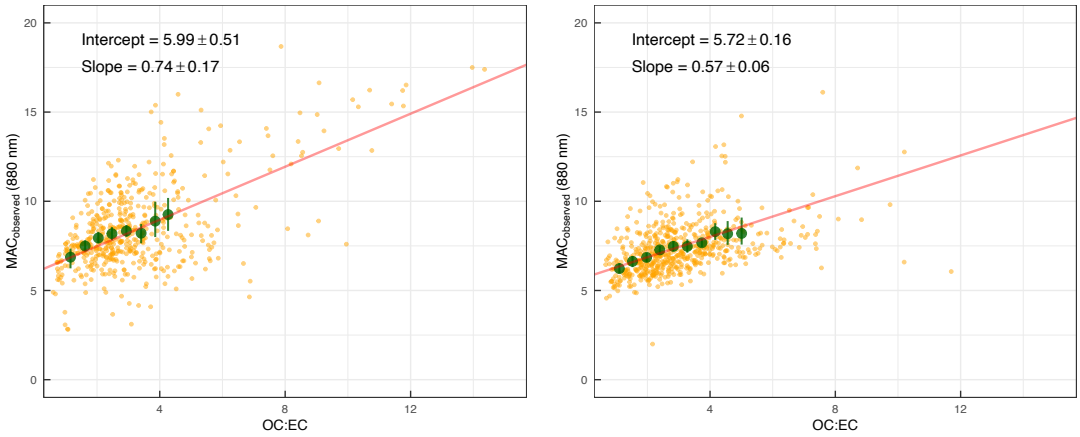

Figure S1: Mass absorption cross-section (MAC) as a function of the online OC-EC ratio at BCN for the AE33 absorption measurement at 880 nm for the a) cold and b) warm period. The intercept obtained with the Deming regression yields the experimental reference MAC of Fig. S3.

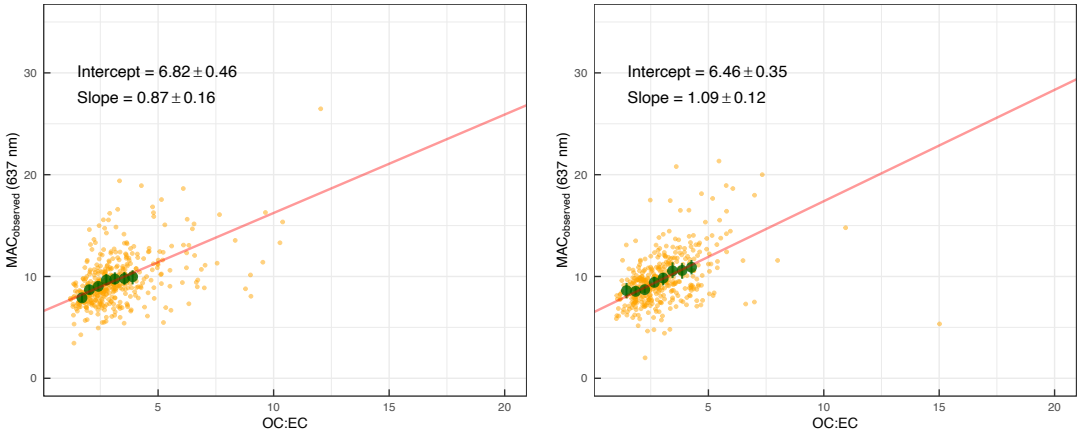

Figure S2: Mass absorption cross-section (MAC) as a function of the offline OC-EC ratio at BCN for the MAAP absorption measurement at 637 nm for the a) cold and b) warm period. The intercept obtained with the Deming regression yields the experimental reference MAC of Fig. S3.

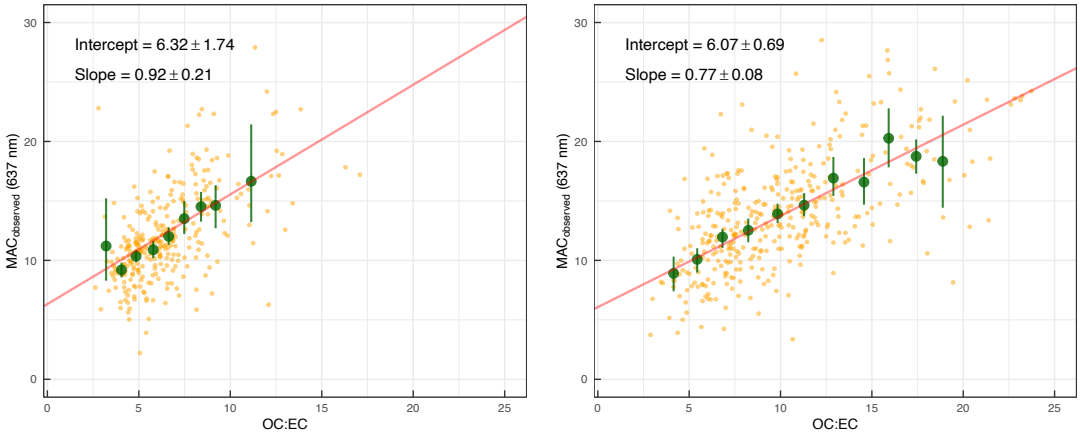

Figure S3: Mass absorption cross-section (MAC) as a function of the offline OC-EC ratio at MSY for the MAAP absorption measurement at 637 nm for the a) cold and b) warm period. The intercept obtained with the Deming regression yields the experimental reference MAC of Fig. S3.

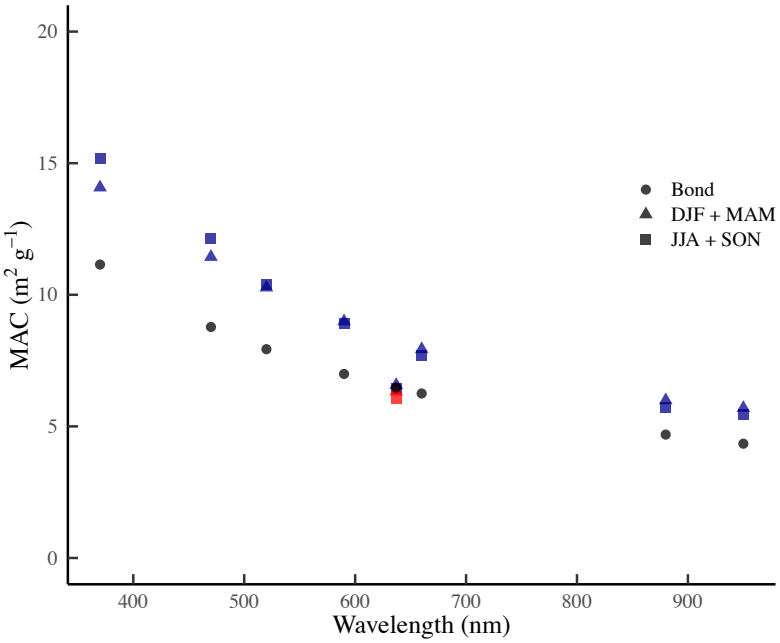

Figure S4: Pure BC MAC ($m^2 g^{-1}$) values obtained from Bond et al. (2006), and experimentally from online techniques via AE33 and Sunset online OC:EC measurements at BCN, and offline via a MAAP at 637 nm and offline OC:EC measurements. BCN station is represented by blue points and Montseny by green points.

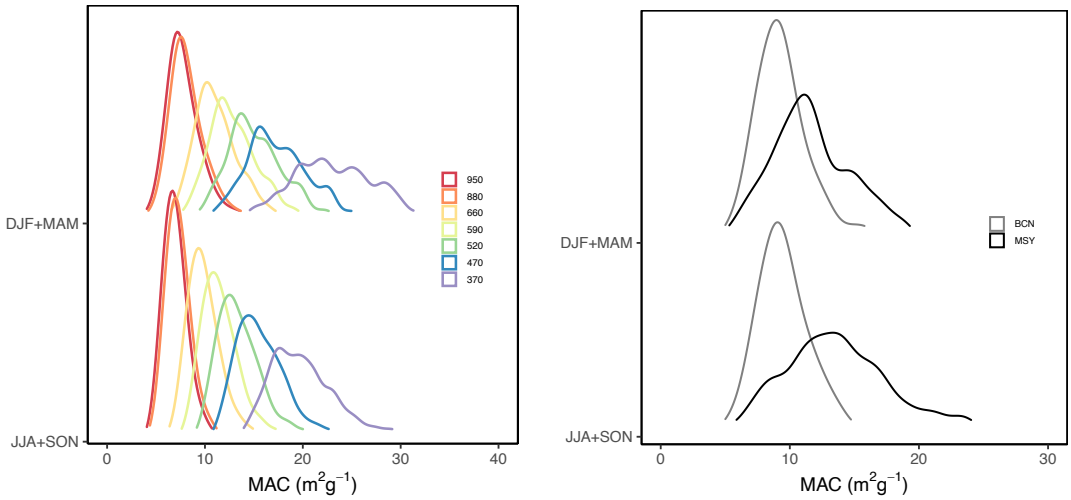

Figure S5: Seasonal frequency distributions of the mass absorption cross-section (MAC) at a) BCN station using a multi-wavelength AE33, and b) at both BCN and MSY at 637 nm using a MAAP.

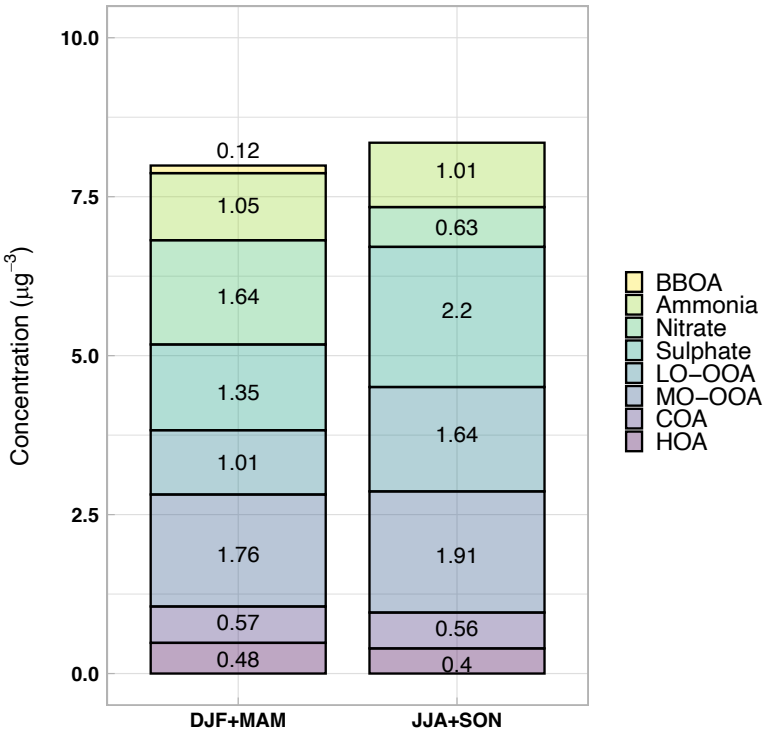

Figure S6: Proportion of the different sources of both organic and inorganic aerosols BCN through-out the seasons during the 2018-2019 period (Via et al., 2021).

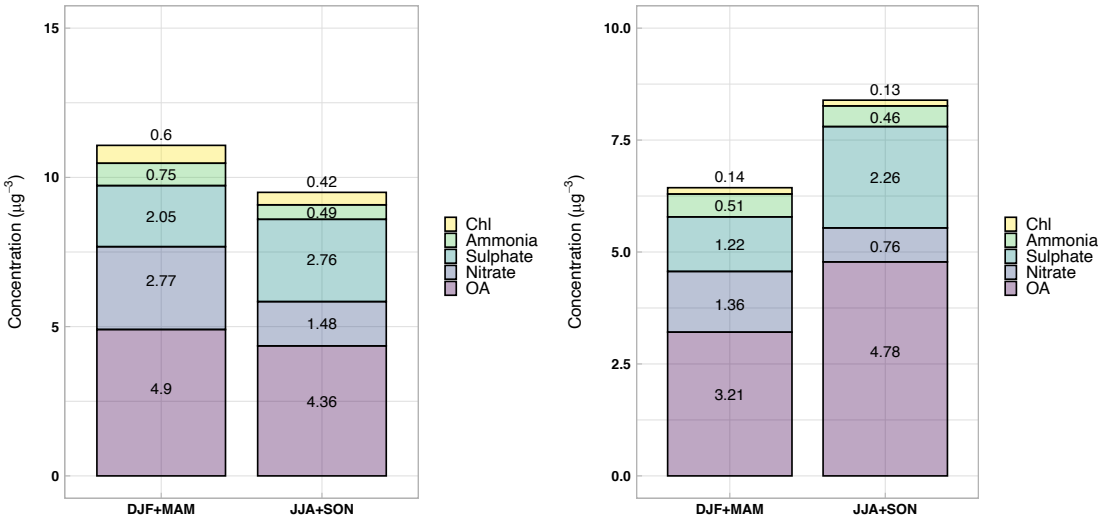

Figure S7: Proportion of the different sources of both organic and inorganic aerosols during the different seasons of the 2011-2018 measurement period at a) BCN, and b) MSY (Veld et al., 2021).

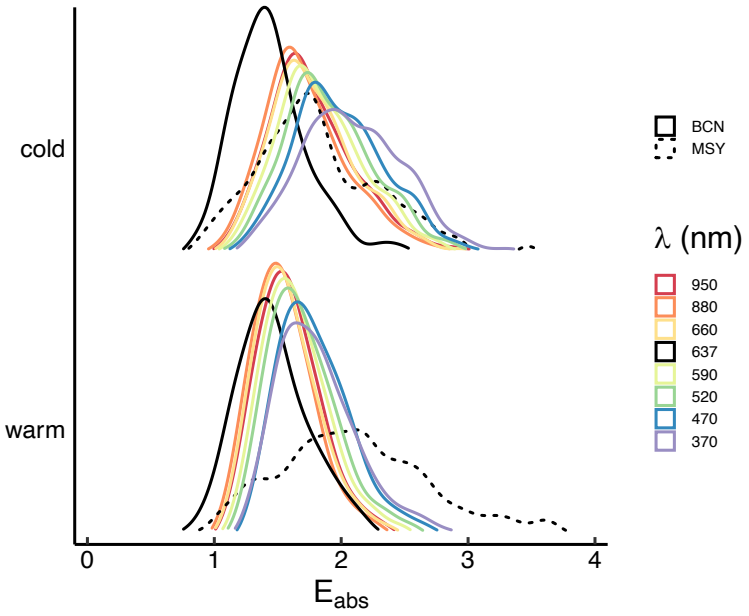

Figure S8: Seasonal frequency distributions of E_{abs} using as a reference MAC the theoretical value provided by Bond et al. (2006) extrapolated to 7 wavelengths measured AE33 wavelengths (370, 470, 520, 590,660, 880 and 950 nm) at BCN station, and to the MAAP wavelength at 637 nm at both BCN and MSY.

Table S1: Absorption enhancement for both external ($E_{abs,ext}$) and internal ($E_{abs,int}$) mixing for both a cold and warm period using the experimental MAC ref value.

	Overall		**Cold season**		**Warm season**	
λ (nm)	**$E_{abs,ext}$**	**$E_{abs,int}$**	**$E_{abs,ext}$**	**$E_{abs,int}$**	**$E_{abs,ext}$**	**$E_{abs,int}$**
370	0.17 ± 0.18	–	0.34 ± 0.17	–	0.06 ± 0.15	–
470	0.10 ± 0.09	–	0.20 ± 0.08	–	0.02 ± 0.09	–
520	0.07 ± 0.07	–	0.14 ± 0.06	–	0.02 ± 0.06	–
590	0.05 ± 0.05	–	0.09 ± 0.05	–	0.02 ± 0.05	–
660	0.03 ± 0.04	–	0.06 ± 0.04	–	0.01 ± 0.03	–
880	–	1.28 ± 0.36	–	1.33 ± 0.43	–	1.25 ± 0.28

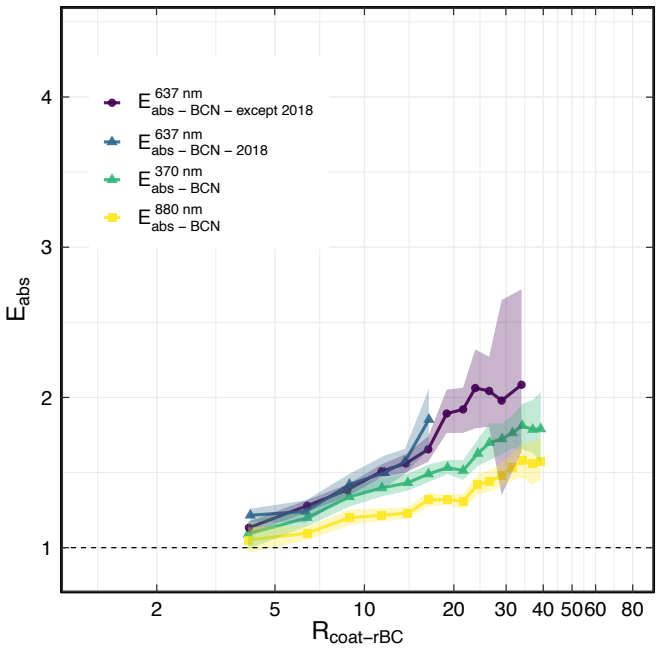

Figure S9: Absorption enhancement, E_{abs}, as a function of the non-refractory PM to EC ratio at BCN station. As in Fig. 3 but omitting the E_{abs} for MSY and showing the values of E_{abs} obtained offline for the MAAP just for 2018 and for all the years except 2018; showcasing the large inter-annual variability.

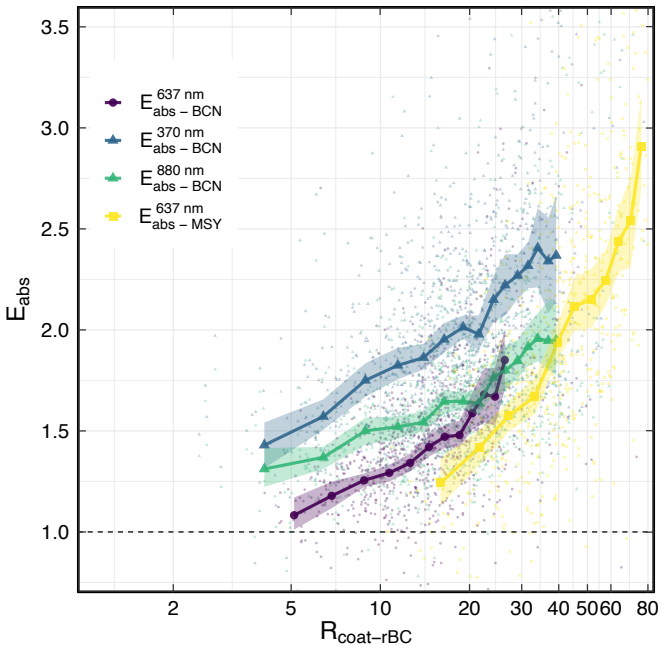

Figure S10: Absorption enhancement, E_{abs}, as a function of the non-refractory PM to EC ratio for BCN and MSY station. As in Fig. 3 but using as a reference MAC the theoretical value provided by Bond et al. (2006) and extrapolating to 370 and 880 nm for the AE33 and online OC:EC and to 637 nm for the MAAP and offline OC:EC.

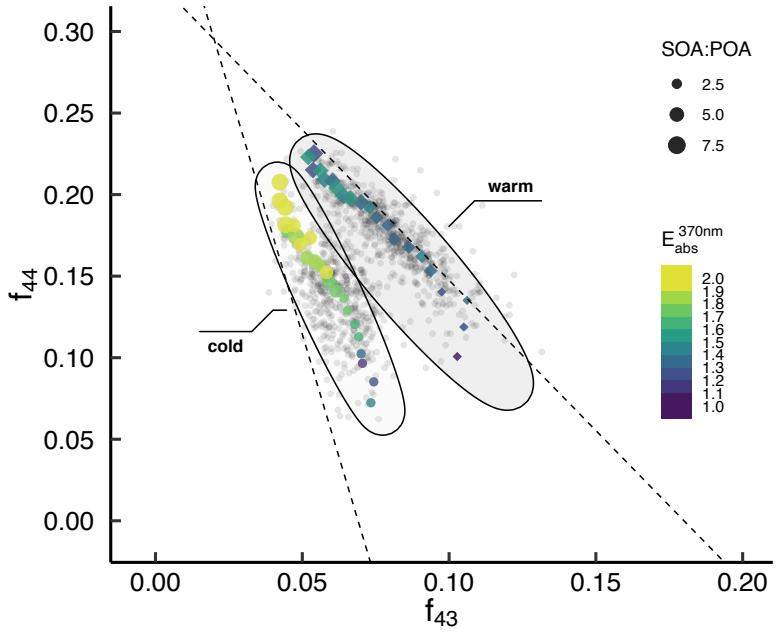

Fig. S11: Absorption enhancement, E_{abs}, at 370 nm at BCN using online measurements as a function of the primary to secondary organic aerosol ratio (POA/SOA), and the atmospheric aging (following Ng. et al., 2010 proposed triangle plot, f_{44} vs f_{43}). The $f_{44}$and f_{43} factors used are the ones presented by Via et al. (2021) for the same time period from the Q-ACSM measurements.

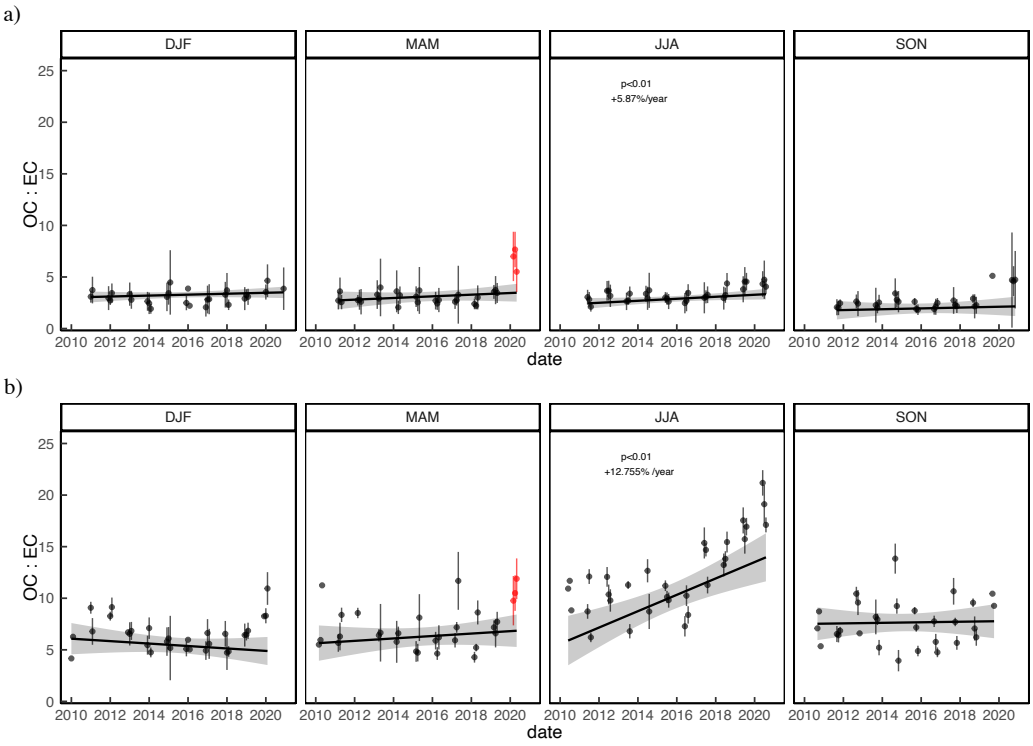

Fig. S12: Seasonal trends of the OC-EC ratio in a) BCN between 2011 and 2020, and b) MSY between 2010 and 2020. COVID-19 lockdown period is marked by the red dots.

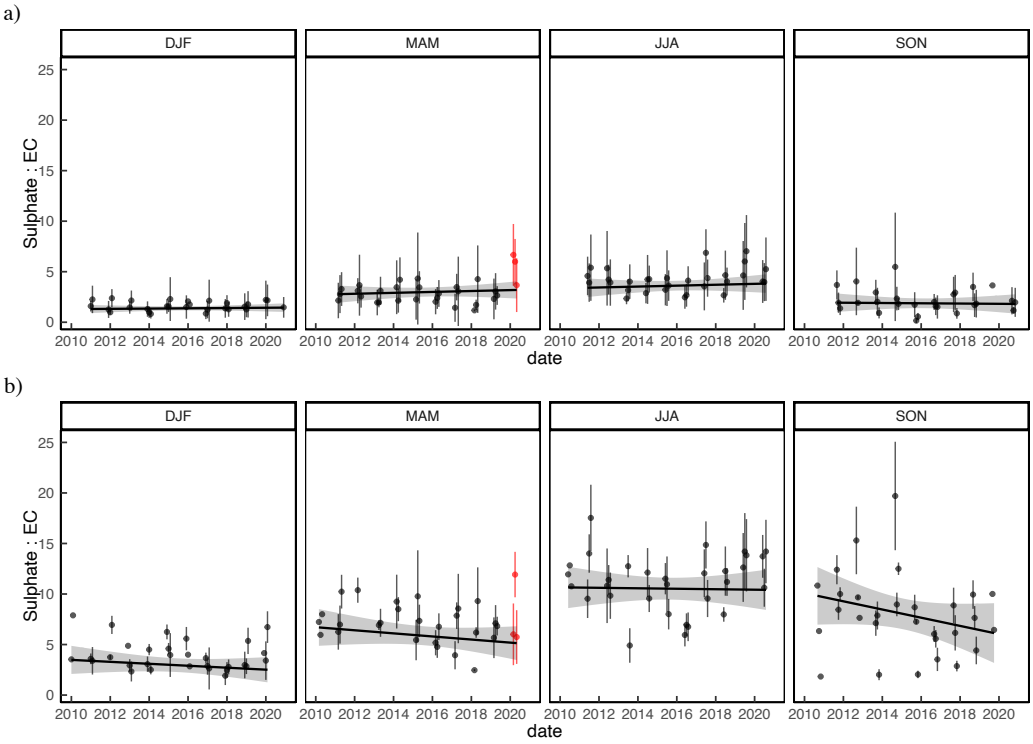

Fig. S13: Seasonal trends of the Sulphate-EC ratio in a) BCN between 2011 and 2020, and b) MSY between 2010 and 2020. COVID-19 lockdown period is marked by the red dots.

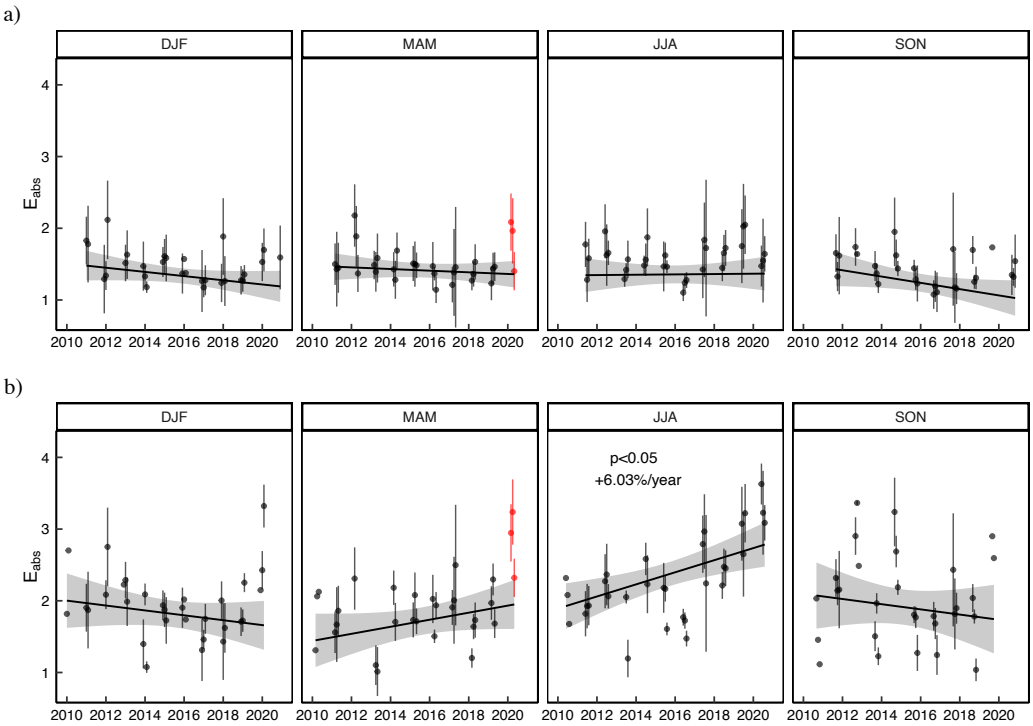

Fig. S14: Absorption enhancement, E_{abs} at 637 nm seasonal trend analysis between 2011 and 2020 at a) Barcelona and b) Montseny station. The trend analysis was performed using a Theil-Sen function over the E_{abs} offline measurements using a theoretical reference MAC (Bond et al., 2006). Dust influenced measurements were excluded. COVID-19 lockdown period is marked by the red dots.